nature nanotechnology

ARTICLES

https://doi.org/10.1038/s41565-019-0609-5

A highly reflective biogenic photonic material from core–shell birefringent nanoparticles

Benjamin A. Palmer[1,2,9*], Venkata Jayasurya Yallapragada[3,9], Nathan Schiffmann[1], Eyal Merary Wormser[4], Nadav Elad[5], Eliahu D. Aflalo[6,7], Amir Sagi[6,8], Steve Weiner[1], Lia Addadi[1] and Dan Oron[3*]

Spectacular natural optical phenomena are produced by highly reflective assemblies of organic crystals. Here we show how the tapetum reflector in a shrimp eye is constructed from arrays of spherical isoxanthopterin nanoparticles and relate the particle properties to their optical function. The nanoparticles are composed of single-crystal isoxanthopterin nanoplates arranged in concentric lamellae around a hollow core. The spherulitic birefringence of the nanoparticles, which originates from the radial alignment of the plates, results in a significant enhancement of the back-scattering. This enables the organism to maximize the reflectivity of the ultrathin tapetum, which functions to increase the eye's sensitivity and preserve visual acuity. The particle size, core/shell ratio and packing are also controlled to optimize the intensity and spectral properties of the tapetum back-scattering. This system offers inspiration for the design of photonic crystals constructed from spherically symmetric birefringent particles for use in ultrathin reflectors and as non-iridescent pigments.

Many spectacular optical phenomena in nature are produced by the interaction of light with structures that exhibit nanoscale variations in refractive index[1,2]. These nanostructures may be arranged in one, two or three-dimensions and exhibit periodic[3,4], quasi-periodic[5] or random[6] variations in their indices of refraction. Iridescent, narrow-band colours are produced by highly periodic systems[3,7], matte non-iridescent colours by partially ordered or disordered systems[5,8–10] and white coloration by light-scattering from randomly arranged objects of size comparable to optical wavelengths[6,11,12]. The brightness of the colours depends on both the index contrast between the materials and on the number of repeats. Thus, the use of high-index materials enables the formation of thinner optical elements.

The highest refractive index materials in biology are crystals of small organic molecules. A common motif for biogenic reflectors is that of multilayer stacks of plate-like crystals interspersed with cytoplasm to form a Bragg reflector[13]. Reflectivity results from the constructive interference of light reflected from the periodic crystal–cytoplasm interfaces. By far the most widespread crystal found in such structures is guanine[14], which is used to produce highly reflective materials for coloration[13,15–18] and vision[19–21]. The utility of guanine as a reflective material derives from its crystal structure, characterized by stacks of planar hydrogen-bonded molecular arrays[22]. The refractive index for light that impinges normal to the hydrogen-bonded planes is $n = 1.83$ (ref. [23]). Aside from guanine, only a few other optically functional organic crystals have been unequivocally identified in nature[24–26]. We recently characterized a previously unknown biogenic crystal in the eyes of decapod crustaceans—the pteridine isoxanthopterin[27]. Similarly to guanine, isoxanthopterin crystals are composed of layers of planar hydrogen-bonded molecular arrays, which leads to an average calculated refractive index within this plane of $n = 1.96$—one the highest refractive indices of any biological material[27].

Decapod crustaceans (for example, lobsters, shrimp and crayfish) possess a reflecting superposition compound eye[28] composed of thousands of eye units called ommatidia. The ommatidia extend from the cornea and terminate in a rhabdom—the photoreceptive unit of the retina (Fig. 1a). The barrel-shaped rhabdoms are constructed from microvilli. The microvilli are protrusions from surrounding retinal cells and are enveloped by the tapetum reflector. The function of the tapetum is: (1) to reflect non-absorbed photons back into the retina to enhance light sensitivity and (2) to prevent cross-talk between adjacent rhabdoms in the retina. We found that the tapetum reflector in several species of decapods is composed of nanoscopic spheres of crystalline isoxanthopterin[27]. Here we investigate the structural and optical properties of these unusual spheres.

The whiteleg shrimp *Litopenaeus vannamei* was selected for study because of the high density of isoxanthopterin nanospheres in its eyes. Here we show that the nanospheres in *L. vannamei* are composed of many oriented single-crystal plates arranged in concentric lamellae around a hollow core. The spherically symmetric birefringence of these nanospheres, which results from the radial alignment of the component crystalline isoxanthopterin nanoplatelets, significantly enhances the back-scattering from the thin tapetum layer. In addition, the size, core/shell ratio and packing of the particles are exquisitely controlled to enhance the performance of this functional unit. Our findings provide a rationalization for the optical functionality of the tapetum and offer inspiration for the development of

[1]Department of Structural Biology, Weizmann Institute of Science, Rehovot, Israel. [2]Present address: Department of Chemistry, Ben-Gurion University of the Negev, Beer-Sheva, Israel. [3]Department of Physics of Complex Systems, Weizmann Institute of Science, Rehovot, Israel. [4]Department of Chemical Engineering, Ben-Gurion University of the Negev, Beer-Sheva, Israel. [5]Department of Chemical Research Support, Weizmann Institute of Science, Rehovot, Israel. [6]Department of Life Sciences, Ben-Gurion University of the Negev, Beer-Sheva, Israel. [7]Department of Life Sciences, Achva Academic College, Arugot, Israel. [8]The National Institute for Biotechnology in the Negev, Ben-Gurion University of the Negev, Beer-Sheva, Israel. [9]These authors contributed equally: Benjamin A. Palmer, Venkata Jayasurya Yallapragada. **One sentence summary**: The birefringence of isoxanthopterin crystalline spherulites enhances the reflectivity of a biological photonic crystal. *e-mail: Bpalmer@bgu.ac.il; Dan.Oron@weizmann.ac.il

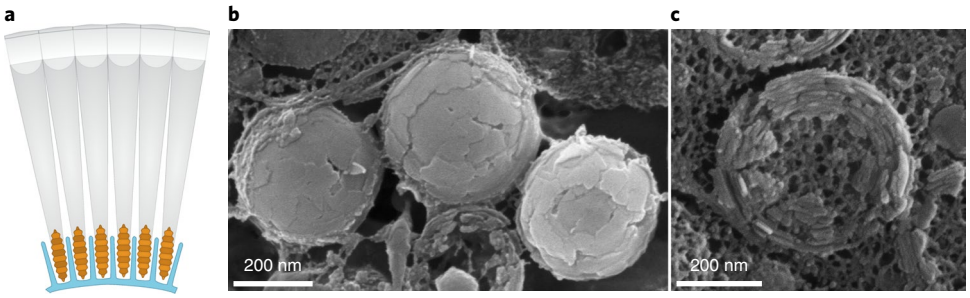

Fig. 1 | Schematic of the eye and in situ images of isoxanthopterin nanoparticles. a, Schematic of a cross-section through a reflecting superposition compound eye showing the ommatidia (transparent grey), rhabdoms (orange) and tapetum reflector (blue) composed of isoxanthopterin nanospheres (**b**,**c**). The tapetum forms an envelope around the lower parts of the rhabdoms. **b**,**c**, Cryo-SEM micrographs of whole (**b**) and fractured (**c**) isoxanthopterin nanoparticles from the eye of *L. vannamei* following high-pressure freezing and freeze fracture.

previously unexplored photonic materials, made from spherically symmetric birefringent particles.

The structural properties of the nanoparticles

The isoxanthopterin particles in the eye of *L. vannamei* are composed of many nanoscale platelets (Fig. 1b,c and Supplementary Figs. 1 and 2) arranged in concentric lamellae around a hollow core (Fig. 1c and Supplementary Figs. 1 and 2). The platelets are irregular planar polygons with dimensions of ca. 50 × 50 × 10 nm (Fig. 1b, Fig. 2c inset and Supplementary Fig. 2). Eight to ten layers of these platelets make up the nanoparticle shell (Fig. 1c). The hollow core of the nanoparticle has a texture similar to that of the surrounding cytoplasm (Fig. 1c), which indicates that it is probably composed of an aqueous medium.

Transmission electron microscopy (TEM) images confirm the hollow nature of the nanoparticles (Fig. 2a), which have an average diameter of 330 nm (±16 nm, $n = 92$), a shell thickness of 70 nm (±7 nm, $n = 53$) with a low polydispersity. Electron diffraction patterns obtained from single nanoparticles exhibit numerous reflections for each d spacing, which demonstrates that the particles comprise many crystals with varying orientations (Fig. 2b). The most intense reflection at a d spacing of ~3.2 Å, the (200) reflection, corresponds to the distance between hydrogen-bonded molecular layers[27]. After vigorous sonication of the extracted nanoparticles (Supplementary Information) and deposition of the resulting suspension on a TEM grid, the grid was covered with individual nanoscopic plates with dimensions and morphologies similar to those of the nanoparticle platelets observed in situ by cryoscanning electron microscopy (cryo-SEM). Electron diffraction patterns of these plates show that they diffract as single crystals (Fig. 2c). The d^* spacings, intensities and symmetry of the pattern are consistent with the (0kl) layer of isoxanthopterin (Supplementary Fig. 3). This demonstrates that the large crystal face is parallel to the (100) crystallographic plane, and consequently to the planar hydrogen-bonded layers of the isoxanthopterin molecules. We can thus conclude that the nanoparticles are composed of single-crystal isoxanthopterin plates, with the a axes of individual platelets projecting radially from the surface of the sphere to form a spherically symmetric birefringent particle. The volume rendering of a single particle reconstructed by TEM tomography (Fig. 2d) reveals individual crystal plates on the particle surface. Images of two-dimensional slices taken at different heights through the lower shell of the particle show lattice fringes with a periodicity of 10.2 Å (Fig. 2e–h), which corresponds to half of the c axis of isoxanthopterin ($c = 19.98$ Å) (Supplementary Fig. 4). Interestingly, the lattice fringes in slices taken from different heights through the shell are aligned in the bc plane. This demonstrates that the nanoparticle shell contains domains of co-oriented crystals that extend throughout the entire shell thickness (Fig. 2g,h, insets). No correlation between the b and c axes orientations in neighbouring domains was observed.

The nanoparticle assemblies

Within the tapetum of *L. vannamei*, the isoxanthopterin nanoparticles are densely packed in membrane-delimited compartments (Fig. 3a,b). The compartments are typically 2–3 µm wide and elongated along the eye's optic axis (Fig. 3). Within these compartments, close-packed, nearly periodic arrays of particles are observed.

On a longer length scale, numerous nanoparticle packets are co-assembled to form an envelope around the lower half of each rhabdom—the photoreceptive unit of the retina (Fig. 3c and also the schematic in Fig. 1a). Although the particles in individual packets are ordered, there is no long-range periodicity in the ordering in adjacent packets. The component nanoparticle packets are arranged in columns that separate adjacent rhabdoms in the retina (Fig. 4a) to form a dense sheath around the seven-lobed rhabdoms (Fig. 4b). Polarizing light micrographs of longitudinal eye sections show that the tapetum reflector is distinctly blue (Fig. 4a,b).

We measured the back-scattering from the tapetum and the underlying pigment layer (Fig. 4c) using an optical microscope by illuminating a small area of these regions and collecting the resulting scattered light with a high numerical aperture objective (Supplementary Materials and Methods). To obtain a qualitative understanding of the variation of reflectivity with wavelength, the measured spectra were divided by the source spectrum. As the spatial extent of each ordered region of nanoparticles is small (~2 µm), a typical measurement of the white-light back-scattering spectrum of the tapetum in a microscope averages over several orientations and angles of incidence. For a completely ordered system, variations in these parameters lead to a change in the position of the reflectivity maxima. Thus, the smooth back-scattered spectrum shown in Fig. 4c represents the relatively isotropic response of the entire nanocrystal arrangement. This measurement also confirms that the tapetum back-scattering is stronger in the blue end of the spectrum. For comparison, we show the scattering spectrum of the underlying pigment layer, which essentially absorbs most of the light that impinges on it (Fig. 4c).

To understand the effect of the unique spherulitic birefringence and of the core/shell ratio of the particles on the reflectivity of the tapetum, we performed numerical computations of (1) scattering from individual particles and (2) reflection from close-packed assemblies of particles.

Optical properties of the nanoparticles and their assemblies

We first consider the optical properties of individual nanospheres. The nanospheres are constructed from single-crystal isoxanthopterin

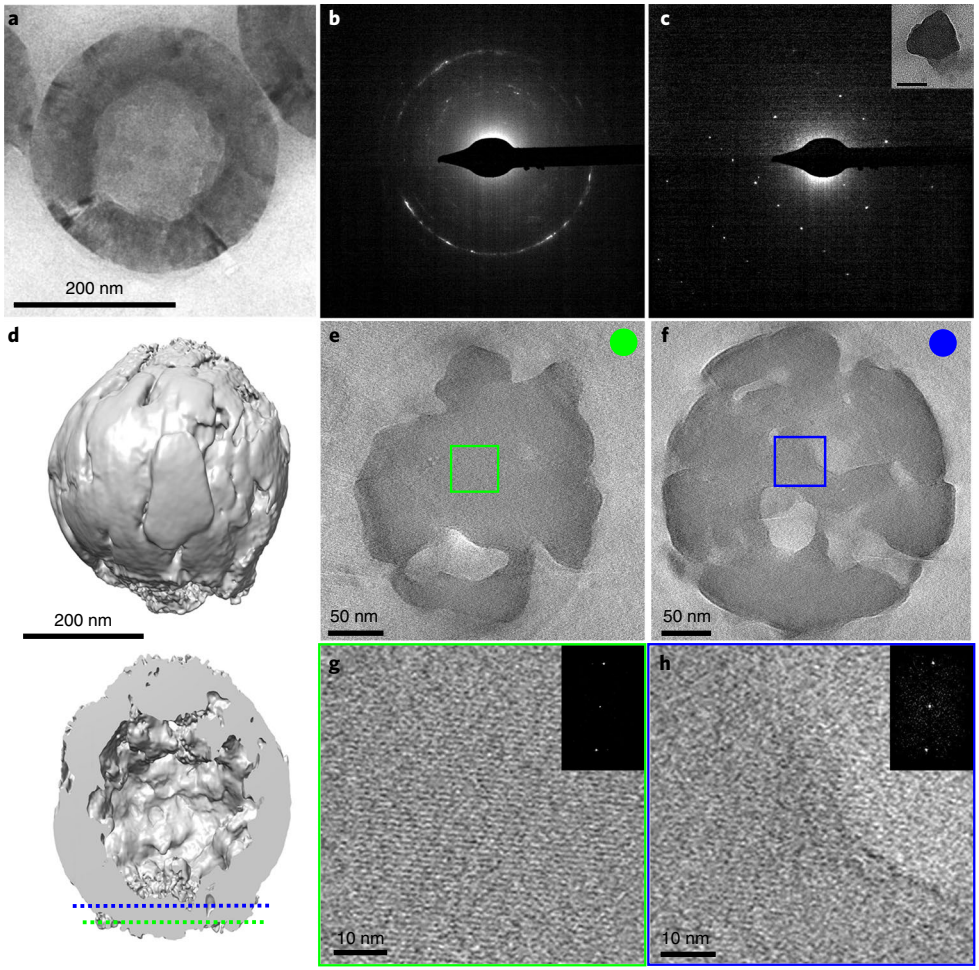

Fig. 2 | The structural properties of the nanoparticles. a, TEM image of an isoxanthopterin nanoparticle from the tapetum of *L. vannamei*. **b**, Electron diffraction pattern of the particle in **a**. **c**, Electron diffraction pattern of a single isoxanthopterin crystal plate on the [0*kl*] zone. Inset: TEM image of the corresponding platelet. Scale bar, 50 nm. **d**, TEM tomogram of a single particle (upper; whole particle, lower; digitally sliced particle showing the particle interior). The dashed green and blue lines indicate the locations of the *xy* planes through the particle shell used for the two-dimensional-slice reconstructions in **e** and **f**, respectively. The particle is artificially elongated along *z* because of the missing wedge in the tomogram. **g**,**h**, High-magnification images of the marked areas in **e** and **f**, respectively (insets show the corresponding fast Fourier transforms).

platelets with the *a* axes of the crystals projecting away from the surface of the sphere. Biogenic isoxanthopterin has an orthorhombic crystal structure and is thus biaxial, possessing three principal refractive indices along the *a*, *b* and *c* directions (calculated as $n_a = 1.40$, $n_b = 2.02$ and $n_c = 1.90$ (ref. [29]). As the refractive indices within the hydrogen-bonded *bc* plane are quite similar, and the *b* and *c* axes are not oriented in neighbouring domains, we treat the nanosphere shell as a uniaxial material with an in-plane ordinary refractive index, n_o, of 1.96 (the average of n_b and n_c) and an out-of-plane extraordinary refractive index, n_e, of 1.40. This low refractive index extraordinary optic axis projects radially outward in all directions. The nanoparticles thus exhibit spherulitic birefringence that possesses the same rotational symmetry as an isotropic sphere (Fig. 5a). For light that impinges on such a nanoparticle, the polarization tangent to the surface of the sphere experiences a particularly high refractive index ($n_o = 1.96$).

We used a modified Mie theory[30–32] to calculate the scattering cross-section of the core–shell nanoparticles as a function of wavelength. We compare the case of a shell made of uniaxial material ($n_o = 1.96$, $n_e = 1.40$) to an effective isotropic shell ($n = 1.78$), the refractive index of which is the average of the three anisotropic refractive indices of crystalline isoxanthopterin. Figure 5b shows that the total scattering cross-section of the anisotropic sphere is only slightly higher than that of the isotropic sphere.

However, a more relevant quantity in the context of the function of the tapetum is the back-scattering efficiency. We calculated this quantity by integrating the scattered intensity over a hemisphere of a 2π solid angle in the backward direction and then normalizing the resulting value by dividing it by the area of the cross-section of a sphere[33] (Supplementary Fig. 5 gives the scattering geometry). The results show that the back-scattered intensity of the birefringent nanosphere is approximately doubled for blue light and even further increased for green and red light relative to that of the isotropic particle (Fig. 5c). To understand the effect of the shell thickness on back-scattering, similar calculations were performed while varying the relative thicknesses of the shell. For the isotropic particle (Fig. 5d), the presence of a low refractive index core in the nanosphere leads to an increased backward scattering in comparison to a solid sphere, and reaches a maximum for a shell thickness of ~70 nm for wavelengths between 350 and 450 nm. For the spherically birefringent nanospheres (Fig. 5e), the backward scattering is significantly enhanced over a broad wavelength range (380– 600 nm) for shell thicknesses of 70 nm or higher, with a maximum again observed at around a 70 nm shell thickness. Most interestingly, this optimum

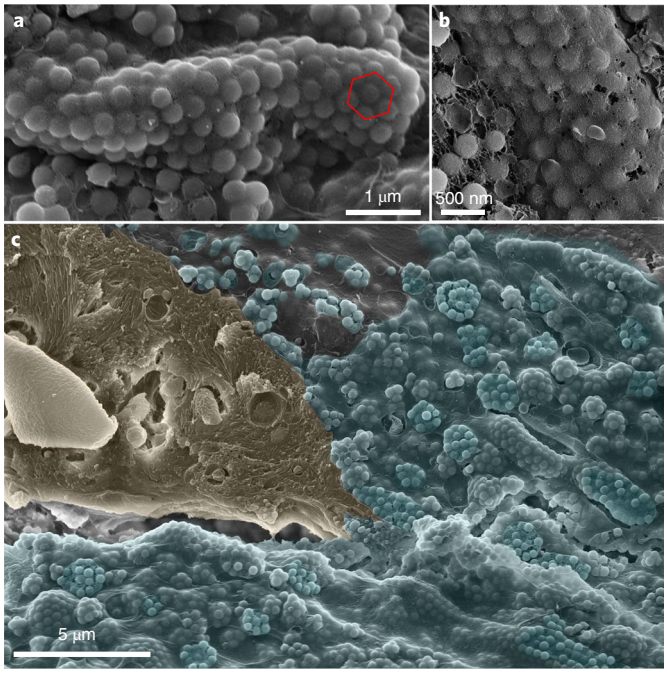

Fig. 3 | Close-packing of isoxanthopterin nanoparticles into compartments and their arrangement within the retina. a,**b**, Cryo-SEM micrographs of hexagonally close-packed nanoparticles in membrane-delimited compartments in the tapetum. The red hexagon highlights the hexagonal packing. **c**, Pseudo-coloured, low-magnification cryo-SEM of a longitudinal section through the retina of *L. vannamei*. The lower part of the rhabdom (orange) comprises microvilli projections that emanate from seven surrounding retinal cells. Nanoparticle packets are pseudo-coloured in blue.

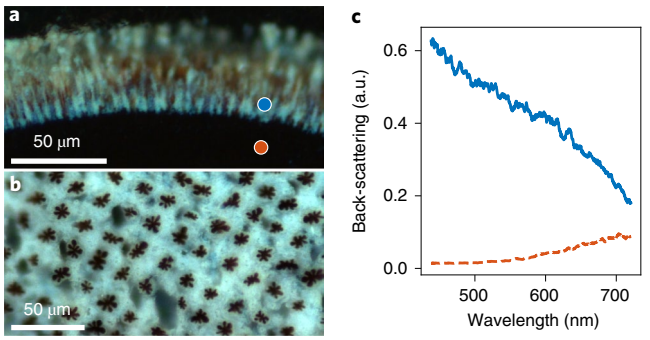

Fig. 4 | The microstructure and optical properties of the tapetum. **a**,**b**, Polarizing optical micrographs of the tapetum viewed perpendicular (**a**) and parallel (**b**) to the optic axis of the eye. The bright-blue structure is the tapetum. The seven-lobed dark features embedded within the tapetum, seen in **b**, are the rhabdoms. **c**, Wavelength dependence of the back-scattering spectrum from the tapetum (blue trace) and pigment (red trace) measured in an optical microscope using unpolarized light at the positions of the blue and red dots (respectively) in **a**. a.u., arbitrary units.

thickness of 70 nm (which maximizes back-scattering using a minimum amount of material) is equivalent to the experimentally observed shell thickness.

As can be seen in Fig. 3, the nanospheres exist as close-packed three-dimensional assemblies that exhibit significant short-range order. Such arrays exhibit strong reflections at specific wavelengths, determined by the periodicity of the structure and the refractive index of the spheres[34]. The periodicity in these assemblies is comparable to the diameter of the particles (~300 nm), which leads to a high reflectivity in the blue end of the visible spectrum. We observe that at the interfaces of the membrane-bound assemblies, the spheres are typically arranged in a hexagonal lattice (Fig. 3), which suggests that the relevant optical interfaces are parallel to the (111) plane of a face-centred cubic (fcc) lattice.

To explore the reflective properties of such close-packed assemblies, we performed finite difference time domain simulations of reflectivity at an interface parallel to the (111) plane of a 3 μm thick fcc lattice of the nanospheres at normal incidence (https://www.lumerical.com/products/fdtd-solutions/) (Supplementary Information). The dependence of the reflectivity on the shell thickness for both the uniaxial and isotropic nanoparticle approximations is shown in Fig. 6a,b. For both approximations, the long-wavelength edge of the high-reflectivity band moves to higher wavelengths as the shell thickness increases. This is consistent with the predictions of a simple effective medium model for layers of spheres parallel to an interface[35]. However, as a result of the higher refractive index modulation in the birefringent spheres, the spectral band for an efficient reflection extends to longer wavelengths than in the isotropic particles[34]. For the isotropic particles we observe negligible reflectivity at wavelengths longer than ~425 nm. The reflectivity spectrum is composed of multiple peaks, due to diffraction from various crystal planes within the lattice. The most interesting aspect of these results is that the band of high reflectivity is widest for a shell thickness of 60–80 nm, similar to the range for the enhanced back-scattering of individual nanospheres (Fig. 5d,e). In this range of shell thicknesses, arrays of birefringent nanospheres reflect 70% of the light between 350 and 450 nm, whereas isotropic spheres reflect only 40% (Fig. 6c). We note that these reflectivity calculations were carried out for an idealized fcc arrangement along the (111) face. In the tapetum, however, we expect the reflectivity spectrum to be broader and smoother, due predominantly to the variability in the orientation of the reflecting interface relative to the periodic arrangement, but also to some disorder and defects within each particle assembly.

Relating nanoparticle structure and assembly to the optical function

The tapetum reflector in the eye of *L. vannamei* is constructed from arrays of spherically symmetric, birefringent core–shell isoxanthopterin nanoparticles. The birefringence results from the radial alignment of the component crystal plates within the shell, with the high in-plane refractive index ($n_o = 1.96$) oriented tangentially to the particle surface. This arrangement enhances the refractive index contrast between the shell and the core for light incident on the particle. Our calculations show that, as a consequence of the variations of refractive index within the shell, individual birefringent particles back-scatter twice as much light as an equivalent isotropic particle. This can be rationalized given the multipole expansion of the scattering coefficient[36]. Therefore, in regions with dense concentrations of these particles, the birefringence would enhance the back-scattering.

The tapetum consists of a tightly packed assembly of particles that exhibit local order. In each ordered region, the particles are arranged in a close-packed lattice. Such a periodic arrangement of particles constitutes a photonic crystal, which reflects the light of specific wavelengths due to interference of diffracted waves from each crystal plane of the assembly. A full computational analysis of the reflectivity of the tapetum would be difficult due to the medium complexity[37]. However, a computational analysis is possible for a close packed arrangement (Fig. 6a,b). It is evident from this calculation that the higher refractive index modulation in the birefringent particle assemblies leads to a widening of the reflection bands relative to the assemblies of isotropic particles[34]. We note that the sharp features present in the calculated reflectivity spectra will be smeared out in the tapetum as a result of variability in the arrangement

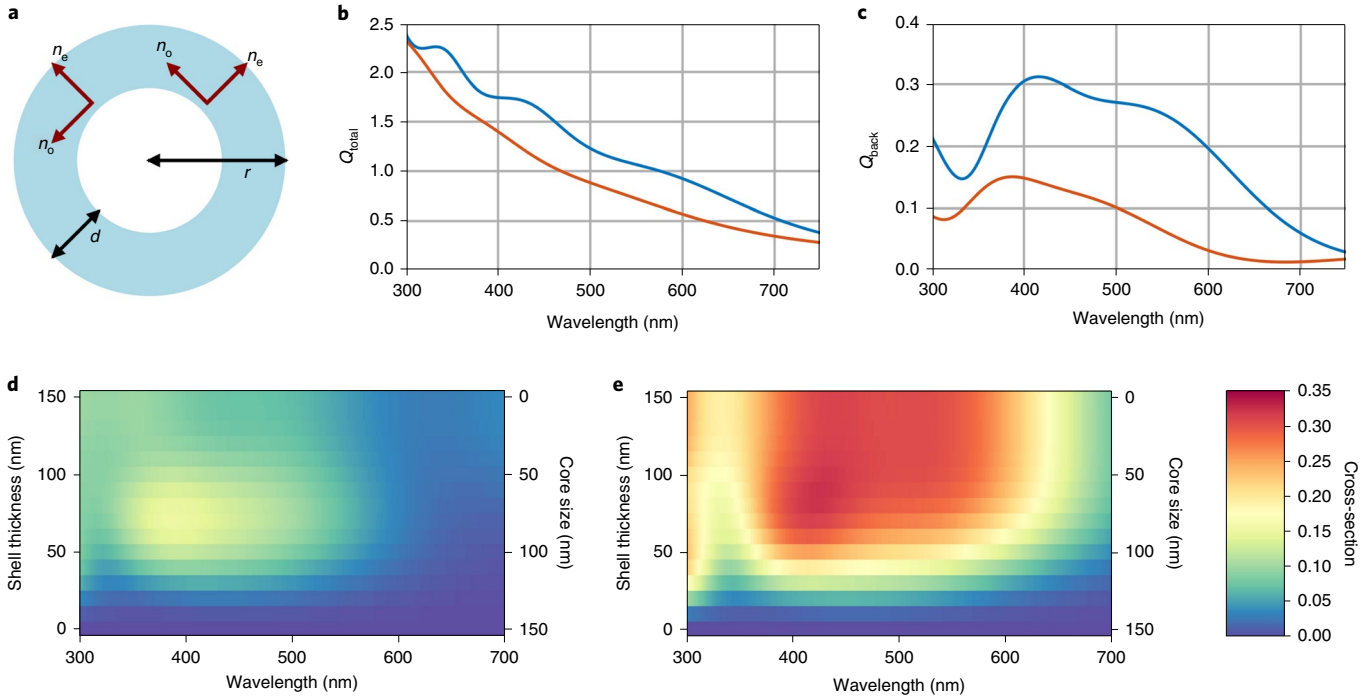

Fig. 5 | Scattering from isolated nanoparticles. a, Schematic of the cross-section of a spherical birefringent nanoparticle. Arrows marked n_e and n_o show the local orientation of the optic axis within the shell. **b**,**c**, Variation of the normalized total scattering cross-section (Q_{total}) (**b**) and normalized back-scattering efficiency (Q_{back}) (**c**) with the wavelengths for a radially anisotropic nanosphere (blue) and an effective isotropic nanosphere (red). The results are for a 300 nm particle with a 70 nm shell thickness and a core with a refractive index of $n_{cytoplasm}$ = 1.33. Normalization was performed by dividing by the physical area of the cross-section of the sphere. **d**,**e**, The variation of the normalized back-scattering cross-section with the shell thickness for an isotropic (**d**) and anisotropic (**e**) shell.

of the particles, and of the orientation of the locally ordered regions[38]. However, we expect the enhancement of reflectivity in birefringent particle assemblies to be present for all orientations, because the birefringence results in increased gaps between the photonic bands[39].

Maximizing the back-scattering efficiency of this material is critical for the function of the shrimp eye, as only a few micrometres of tapetum material separate adjacent rhabdoms in the retina. The rhabdoms must be isolated from each other to prevent 'optical cross-talk', which results in image blurring[27,40,41]. In principle, using thinner layers of reflective material between photoreceptors also enables a higher packing density of photoreceptors, which conceivably improves the spatial resolution of vision. The shrimp appears to have evolved both the component nanoparticles and their ultrastructure to enable the formation of such an ultrathin reflective layer.

In addition to birefringence, the core/shell ratio, size and packing of the particles also appear to be optimized to improve the functionality of the tapetum. The experimentally observed shell thickness of 70 nm is an optimum for obtaining the maximum back-scattering and reflectivity and lowering the sensitivity to small variations in size or shell thickness. The size of the particles is also optimal to preferentially back-scatter the blue light that penetrates the shrimp's habitat (up to 70 m depth[42]). Interestingly, our calculations show that for ordered assemblies of isotropic particles, there is negligible reflectivity above 425 nm, whereas for birefringent particles the reflectivity extends to >450 nm, which broadens the spectral range of reflected light that is effectively absorbed by the shrimp's photoreceptors (which absorb between 400 and 550 nm) (ref. [43]).

The attractive optical properties of the tapetum reflector emerge from the ability of the organisms to control the structural properties of the material at multiple length scales, from the crystal structure, morphology and orientation at the nanometre scale to the particle structure and packing at the micrometre scale. At the smallest length scale, the individual isoxanthopterin platelets are highly ordered single crystals (Fig. 2c). The extremely high calculated refractive index of the crystalline isoxanthopterin derives from the high polarizability of the delocalized π electrons within the hydrogen-bonded molecular layers of the crystal. The thin-plate crystal morphology of biogenic isoxanthopterin is strikingly different from the theoretically predicted growth form[29] and facilitates the formation of a spherical nanoparticle. In the biogenic crystals, the (100) crystal face, parallel to the high in-plane refractive index (n_o), is preferentially expressed and oriented towards the impinging light by virtue of the radial arrangement of the crystallites around the sphere. This arrangement dramatically enhances the reflectivity of the particles. In contrast, the most stable theoretically predicted habit is a prismatic habit, in which the highly reflective (100) face is expressed only as a very minor facet[29]. These observations show that the biological crystallization process is highly controlled, which in turn raises the fascinating question of how crystal formation and assembly occur inside the organism.

Previously, theoretical studies revealed some of the superior optical properties of photonic structures made from birefringent building blocks[44,45], which could not be constructed experimentally because of the difficulties of co-orienting the component uniaxial birefringent particles. The 'genius' of the shrimp solution is in the spherical symmetry of the birefringence, which obviates the need for co-orientation of the optical axes. Such spherically birefringent materials have rarely been considered previously and the shrimp represents a unique example of a natural photonic system that exhibits optical properties not explored before synthetically. Furthermore, we note that due to the inherent disorder in the arrangement the nanoparticles, the tapetum exhibits a smooth

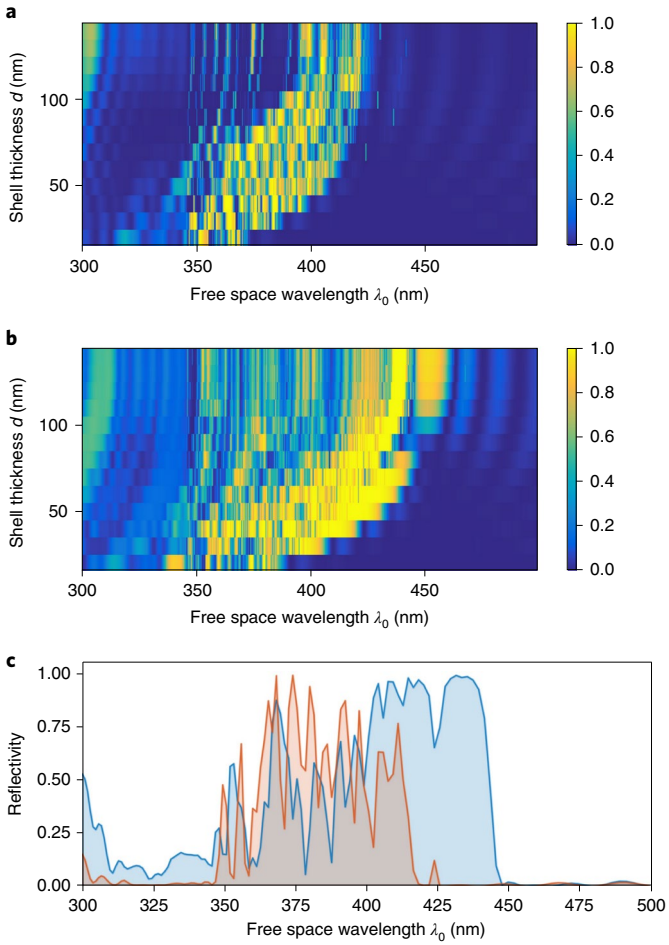

Fig. 6 | Reflectivity from arrays of nanospheres. a, Reflectivity (summed over all reflected diffraction orders and averaged over two orthogonal polarizations) from an interface parallel to the (111) plane of a fcc lattice of core–shell nanospheres, whose shells are made of an isotropic dielectric (n=1.78), for varying shell thicknesses. **b**, Same as **a**, but for spherically birefringent nanospheres made of a uniaxial shell material (n_o=1.96, n_e=1.40). **c**, Reflectivity spectra for the experimentally observed shell thickness of 70 nm from **a** and **b** plotted alongside each other, and binned for clearer visualization. The increased broadband reflectance of the birefringent structure (blue) in the 380–450 nm band (violet–blue) compared to the effective isotropic nanosphere array (red) is clearly observed.

reflectivity spectrum which is not iridescent. These biogenic isoxanthopterin nanoparticles thus offer inspiration for the design of new optical materials that utilize ultrathin reflective layers or non-iridescent structural colours (for example, photonic films, paints, coatings and digital displays[46]). The theoretical work presented here shows how the photonic properties of such devices may be tuned by controlling the structural and material properties of spherically symmetric birefringent particles.

Conclusions

We show that the tapetum reflector of the *L. Vannamei* shrimp, constructed from highly birefringent crystalline isoxanthopterin nanoparticles, displays photonic properties previously unexplored in synthetic systems. The spherically symmetric birefringence of the nanospheres, which results from the radial alignment of component nanoplatelets, causes a dramatic enhancement in the back-scattering both from individual nanospheres and nanoparticle assemblies. The enhanced back-scattering enables the organism to maximize the reflectivity of the ultrathin tapetum layer, which serves to increase the sensitivity of the eye and preserve visual acuity. The size, core/shell ratio and particle packing are also optimized to maximize the back-scattering of the tapetum reflector, both in terms of the intensity and spectral properties. The shrimp system provides inspiration for the design of hitherto unexplored photonic structures made from particles that exhibit spherulitic birefringence.

Online content

Any methods, additional references, Nature Research reporting summaries, source data, extended data, supplementary information, acknowledgements, peer review information; details of author contributions and competing interests; and statements of data and code availability are available at https://doi.org/10.1038/s41565-019-0609-5.

Received: 23 April 2019; Accepted: 2 December 2019;
Published online: 13 January 2020

References

1. Kinoshita, S., Yoshioka, S. & Miyazaki, J. The physics of structural colors. *Rep. Prog. Phys.* **71**, 2–30 (2008).
2. Parker, A. R. 515 million years of structural colour. *J. Opt. A* **2**, R15 (2000).
3. Vukusic, P. & Sambles, J. R. Photonic structures in biology. *Nature* **424**, 852–855 (2003).
4. Ling, L. et al. A highly conspicuous mineralized composite photonic architecture in the translucent shell of the blue-rayed limpet. *Nat. Commun.* **6**, 6322 (2015).
5. Noh, H. et al. How noniridescent colors are generated by quasi-ordered structures of bird feathers. *Adv. Mater.* **22**, 2871–2880 (2010).
6. Vukusic, P., Hallam, B. & Noyles, J. Brilliant whiteness in ultrathin beetle scales. *Science* **315**, 348 (2007).
7. Vignolini, S. et al. Pointillist structural color in *Pollia* fruit. *Proc. Natl Acad. Sci. USA* **109**, 15712–15715 (2012).
8. Harun-Ur-Rashid, M. et al. Angle-independent structural color in colloidal amorphous arrays. *ChemPhysChem* **11**, 579–583 (2010).
9. Forster, J. D. et al. Biomimetic isotropic nanostructures for structural coloration. *Adv. Mater.* **22**, 2939–2944 (2010).
10. Saranathan, V. et al. Structure and optical function of amorphous photonic nanostructures from avian feather barbs: a comparative small angle X-ray scattering (SAXS) analysis of 230 bird species. *J. R. Soc. Interface* **9**, 2563–2580 (2012).
11. Burresi, M. et al. Bright-white beetle scales optimise multiple scattering of light. *Sci. Rep.* **4**, 6075 (2014).
12. Mäthger, L. M. et al. Bright white scattering from protein spheres in color changing, flexible cuttlefish skin. *Adv. Func. Mater.* **23**, 3980–3989 (2013).
13. Denton, E. J. & Land, M. F. Mechanism of reflexion in silvery layers of fish and cephalopods. *Proc. R. Soc. Lond. B* **178**, 43–61 (1971).
14. Gur, D., Palmer, B. A., Weiner, S. & Addadi, L. Light manipulation by guanine crystals in organisms: biogenic scatterers, mirrors, multilayer reflectors and photonic crystals. *Adv. Func. Mater.* **27**, 1603514 (2017).
15. Jordan, T. M., Partridge, J. C. & Roberts, N. W. Non-polarizing broadband multilayer reflectors in fish. *Nat. Photon.* **6**, 759–763 (2012).
16. Gur, D. et al. The mechanism of color change in the neon tetra fish: a light-induced tunable photonic crystal array. *Angew. Chem. Int. Ed.* **54**, 12426–12430 (2015).
17. Gur, D. et al. Structural basis for the brilliant colors of the Sapphirinid copepods. *J. Am. Chem. Soc.* **137**, 8408–8411 (2015).
18. Teyssier, J., Saenko, S. V., van der Marel, D. & Milinkovitch, M. C. Photonic crystals cause active colour change in chameleons. *Nat. Commun.* **6**, 6368–6375 (2015).
19. Palmer, B. A. et al. The image-forming mirror in the eye of the scallop. *Science* **358**, 1172–1175 (2017).
20. Palmer, B. A., Gur, D., Weiner, S., Addadi, L. & Oron, D. The organic crystalline materials of vision: structure–function considerations from the nanometer to the millimeter scale. *Adv. Mater.* **30**, 1800006 (2018).
21. Hirsch, A. et al. Biologically controlled morphology and twinning in guanine crystals. *Angew. Chem. Int. Ed.* **56**, 9420–9424 (2017).
22. Hirsch, A. et al. 'Guanigma': the revised structure of biogenic anhydrous guanine. *Chem. Mat.* **27**, 8289–8297 (2015).
23. Huxley, A. F. High-power interference microscope. *J. Physiol. (Lond.)* **125**, 11–13 (1954).
24. Bohm, A. & Pass, G. The ocelli of Archaeognatha (Hexapoda): functional morphology, pigment migration and chemical nature of the reflective tapetum. *J. Exp. Biol.* **219**, 3039–3048 (2016).

25. Pirie, A. Crystals of riboflavin making up the tapetum lucidum in the eye of a lemur. *Nature* **183**, 985–986 (1959).
26. Caveney, S. Cuticle reflectivity and optical activity in scarab beetles: the role of uric acid. *Proc. R. Soc. Lond. B* **201**, 179–189 (1971).
27. Palmer, B. A. et al. Optically functional isoxanthopterin crystals in the mirrored eyes of decapod crustaceans. *Proc. Natl Acad. Sci. USA* **115**, 2299–2304 (2018).
28. Vogt, K. Zur Optik des Flusskrebsauges. *Z. Naturforsch.* **30c**, 691 (1975).
29. Hirsch, A. et al. Structure and morphology of light-reflecting synthetic and biogenic polymorphs of isoxanthopterin: a comparison. *Chem. Mater.* **31**, 4479–4489 (2019).
30. Roth, J. & Dignam, M. J. Scattering and extinction cross sections for a spherical particle coated with an oriented molecular layer. *J. Opt. Soc. Am.* **63**, 308–311 (1973).
31. Hahn, D. K. & Aragón, S. R. MIE scattering from anisotropic thick spherical shells. *J. Chem. Phys.* **101**, 8409–8417 (1994).
32. Qiu, C. W., Gao, L., Joannopoulos, J. D. & Soljačić, M. Light scattering from anisotropic particles: propagation, localization, and nonlinearity. *Laser Photonics Rev.* **4**, 268–282 (2010).
33. Bohren, C. F. & Huffman, D. R. *Absorption and Scattering of Light by Small Particles* (John Wiley & Sons, 2008).
34. Joannopoulos, J. D., Johnson, S. G., Winn, J. N. & Meade, R. D. *Photonic Crystals: Molding the Flow of Light* 2nd edn (Princeton Univ. Press, 2011).
35. Schroden, R. C., Al-Daous, M., Blanford, C. F. & Stein, A. Optical properties of inverse opal photonic crystals. *Chem. Mater.* **15**, 3305–3315 (2002).
36. Naraghi, R. R., Sukhov, S. & Dogariu, A. Directional control of scattering by all-dielectric core–shell spheres. *Opt. Lett.* **40**, 585–588 (2015).
37. Balestreri, A., Andreani, L. C. & Agio, M. Optical properties and diffraction effects in opal photonic crystals. *Phys. Rev. E* **74**, 036603 (2006).
38. Astratov, V. N. et al. Interplay of order and disorder in the optical properties of opal photonic crystals. *Phys. Rev. B* **66**, 13 (2002).
39. Yallapragada, V. J. & Oron, D. Optical properties of spherulite opals. *Opt. Lett.* **44**, 5860–5863 (2019).
40. Warrant, E. J. & McIntyre, P. D. Strategies for retinal design in arthropod eyes of low F-number. *J. Comp. Physiol. A* **168**, 499–512 (1991).
41. Bryceson, K. P. & McIntyre, P. Image quality and acceptance angle in a reflecting superposition eye. *J. Comp. Physiol. A* **151**, 367–380 (1983).
42. Holthuis, L. B. *Shrimps and Prawns of the World. An Annotated Catalogue of Species of Interest to Fisheries* Vol. 1 (FAO, 1980).
43. Matsuda, K. & Wilder, M. N. Difference in light perception capability and spectral response between juveniles and sub-adults of the whiteleg shrimp *Litopenaeus vannamei* as determined by electroretinogram. *Fish. Sci.* **76**, 633–641 (2010).
44. Zabel, I. H. H. & Stroud, D. Photonic band structures of optically anisotropic periodic arrays. *Phys. Rev. B* **48**, 5004–5012 (1993).
45. Zhi-Yuan, L., Wang, J. & Gu, B.-Y. Creation of partial band gaps in anisotropic photonic-band-gap structures. *Phys. Rev. B* **58**, 3721–3729 (1998).
46. Park, J. et al. Full-spectrum photonic pigments with non-iridescent structural colors through colloidal assembly. *Angew. Chem. Int. Ed.* **53**, 2899–2903 (2014).

Data availability

The data that support the findings of this study are available from the corresponding authors upon reasonable request.

Acknowledgements

This work was supported by Israel Science Foundation Grants 354/18 and 583/17, the Crown Center of Photonics and the ICORE: The Israeli Center of Research Excellence 'Circle of Light.' L.A. is the incumbent of the Dorothy and Patrick Gorman Professorial Chair of Biological Ultrastructure. D.O. is the incumbent of the Harry Weinrebe Professorial Chair of laser physics. B.A.P. is the recipient of the 2019 Azrieli Faculty Fellowship.

Author contributions

B.A.P., S.W., L.A. and D.O. designed and directed the study. V.J.Y. carried out the scattering and reflectivity calculations and performed reflectivity measurements. N.S. and E.M.W. prepared the samples for cryo-SEM and TEM, and performed image analysis and optical microscopy measurements. B.A.P. performed cryo-SEM and optical microscopy measurements. N.E. performed the TEM measurements and TEM tomography analysis. A.S. and E.D.A. provided the specimens and knowledge of shrimp biology. B.A.P., V.J.Y., S.W., L.A. and D.O. wrote the manuscript with contributions from all the authors.

Competing interests

The authors declare no competing interests.

Additional information

Supplementary information is available for this paper at https://doi.org/10.1038/s41565-019-0609-5.

Correspondence and requests for materials should be addressed to B.A.P. or D.O.

Reprints and permissions information is available at www.nature.com/reprints.